

Global Biogeochemical Cycles®

RESEARCH ARTICLE

10.1029/2021GB007192

Key Points:

- Regions at higher risk of coastal hypoxia in the northern Indian Ocean are identified using coastal oxygen observations
- The Indian Ocean Dipole (IOD) can amplify or suppress the seasonal risk of hypoxia by modulating coastal upwelling/downwelling
- The risk is most amplified during positive IOD phases along the coast of the eastern Bay of Bengal

Supporting Information:

Supporting Information may be found in the online version of this article.

Correspondence to:

J. Pearson,
jennap@princeton.edu

Citation:

Pearson, J., Resplandy, L., & Poupon, M. (2022). Coastlines at risk of hypoxia from natural variability in the northern Indian Ocean. *Global Biogeochemical Cycles*, 36, e2021GB007192. <https://doi.org/10.1029/2021GB007192>

Received 15 SEP 2021

Accepted 27 MAY 2022

Coastlines at Risk of Hypoxia From Natural Variability in the Northern Indian Ocean

Jenna Pearson¹ , Laure Resplandy^{1,2} , and Mathieu Poupon¹ 

¹Department of Geosciences, Princeton University, Princeton, NJ, USA, ²High Meadows Environmental Institute, Princeton University, Princeton, NJ, USA

Abstract Coastal hypoxia—harmfully low levels of oxygen—is a mounting problem that jeopardizes coastal ecosystems and economies. The northern Indian Ocean is particularly susceptible due to human-induced impacts, vast naturally occurring oxygen minimum zones, and strong variability associated with the seasonal monsoons and interannual Indian Ocean Dipole (IOD). We assess how *natural* factors influence the risk of coastal hypoxia by combining a large set of oxygen measurements with satellite observations to examine how the IOD amplifies or suppresses seasonal hypoxia tied to the Asian Monsoon. We show that on both seasonal and interannual timescales hypoxia is controlled by wind- and coastal Kelvin wave-driven upwelling of oxygen-poor waters onto the continental shelf and reinforcing biological feedbacks (increased subsurface oxygen demand). Seasonally, the risk of hypoxia is highest in the western Arabian Sea in summer/fall (71% probability of hypoxia). Major year-to-year impacts attributed to the IOD occur during positive phases along the eastern Bay of Bengal (EBoB), where the risk of coastal hypoxia increases from moderate to high in summer/fall (21%–46%) and winter/spring (31%–42%), and along the eastern Arabian Sea (i.e., India, Pakistan) where the risk drops from high to moderate in summer/fall (53%–34%). Strong effects are also seen in the EBoB during negative IOD phases, when the risk reduces from moderate to low year-round (~25% to ~5%). This basin-scale mapping of hypoxic risk is key to aid national and international efforts that monitor, forecast, and mitigate the impacts of hypoxia on coastal ecosystems and ecosystem services.

Plain Language Summary Coastal “dead zones,” with vanishingly low oxygen levels, stress marine organisms, compress their habitats, threaten the sustainability of fisheries, and can lead to mass mortality of marine life. The northern Indian Ocean is particularly vulnerable due to natural physical processes that bring oxygen-poor water onto the continental shelf from vast offshore regions of low-oxygen, and biological processes that can intensify coastal dead zones. Alongside these natural processes, coastal dead zones in the Indian Ocean are also influenced by human activity, such as fertilizer use and waste water management. In this study we use a large set of observations in the northern Indian Ocean to quantify how *natural processes* trigger coastal dead zones seasonally, and how they increase or decrease the risk of coastal dead zones from year-to-year. This information, on where and when coastal dead zones are most likely to occur, is key to anticipate and mitigate impacts on ecosystems and economies.

1. Introduction

Lack of oxygen is one of the most pressing threats to coastal marine ecosystems (Laffoley & Baxter, 2019; Levin et al., 2009). Reports of coastal hypoxia, also called “dead zones,” where nearshore oxygen values fall below 61 µmol/kg (\approx 63 µM, 2 mg/l, or 1.5 ml/l), have increased exponentially over the last few decades, impacting more than 245,000 square kilometers of the coastal ocean (Breitburg et al., 2018; Diaz & Rosenberg, 2008; Gilbert et al., 2010; Vaquer-Sunyer & Duarte, 2008). Hypoxic waters shape the biogeography of benthic and pelagic ecosystems by influencing the physiology and behavior of these communities (e.g., Deutsch et al., 2020; Vaquer-Sunyer & Duarte, 2008). Severe effects include metabolic depression, migration of macro-organisms, and mortality from exposure to low-oxygen conditions (Diaz & Rosenberg, 1995; Ekau et al., 2010; Gray et al., 2002; Levin et al., 2009; Riedel et al., 2008; Roman et al., 2019; Stramma et al., 2010; Vaquer-Sunyer & Duarte, 2008; Wu, 2002; Yoann et al., 2019). In addition, lack of oxygen can alter predator-prey relations (Decker et al., 2004; Nestlerode & Diaz, 1998), disturb bioturbation (Norkko et al., 2015; Villnäs et al., 2013), promote coastal water-column denitrification and nitrous oxide production (Bianchi et al., 2018; Naqvi et al., 2006; Sarkar et al., 2020), and severely impact fisheries (Díaz et al., 2010; Glaspie et al., 2019; Laffoley & Baxter, 2019; Thambithurai et al., 2019). For instance, in 2001 a coastal dead zone collapsed local shrimp fisheries along the

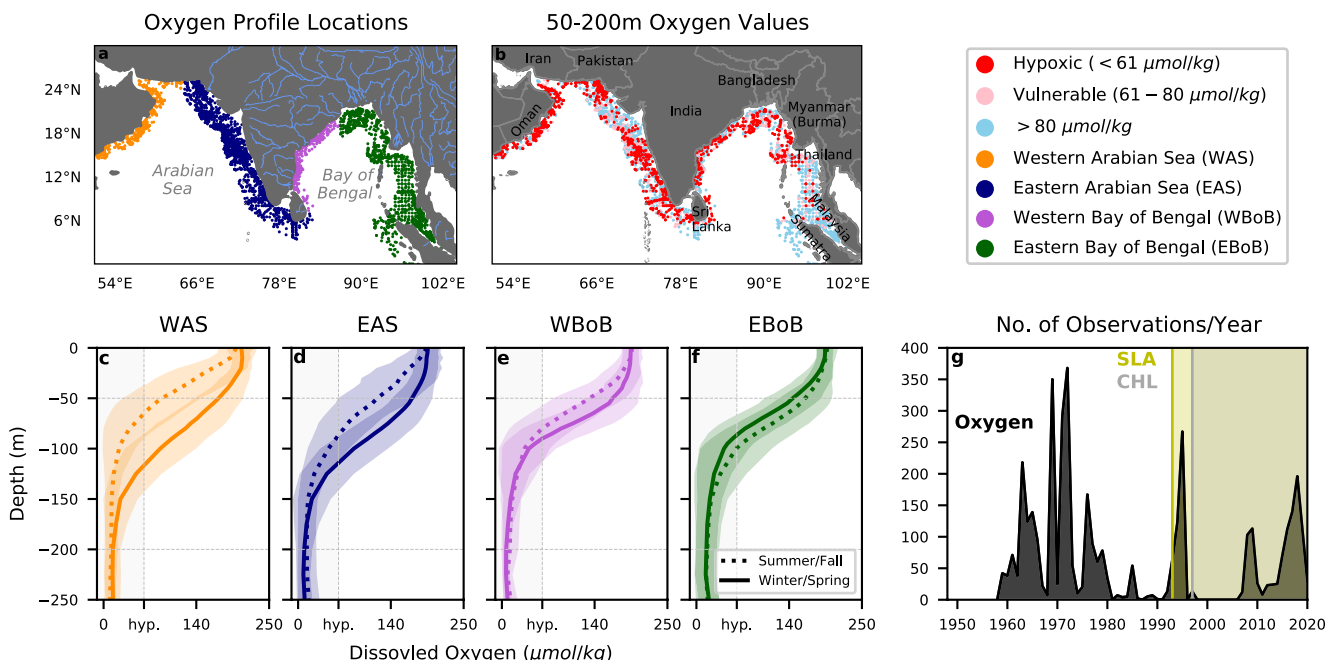


Figure 1. World Ocean Database oxygen profiles (a) locations with data available between 50 and 200 m, and (b) average 50–200 m values identifying hypoxic and vulnerable coastal oxygen values. (c–f) Mean winter/spring (solid) and summer/fall (dotted) profiles for each region, with shading indicating ± 1 spatiotemporal standard deviation and vertical gray dashed lines the hypoxia threshold. (g) Number of profiles per year from 1958 to 2020 overlaid with observational periods for satellite sea level anomaly (SLA, 1993–2020 in yellow) and chlorophyll-a (CHL, 1997–2020 in gray). Colors in (a) indicate the regions used in this study: the western Arabian Sea (WAS), eastern Arabian Sea (EAS), western Bay of Bengal (WBoB) and eastern Bay of Bengal (EBoB). Major river systems are shown in (a).

western coast of India, resulting in a near 5-fold decline in prawn catch compared to 1997, when less hypoxic conditions prevailed (Naqvi et al., 2009). Anticipating when and where low-oxygen conditions are likely to occur, and incorporating this into fisheries management strategies could help maintain sustainable yields. For example, reducing allowable catch rates during hypoxic periods could compensate for expected lower populations (Laffoley & Baxter, 2019).

The Indian Ocean is particularly vulnerable to coastal hypoxia (Figures 1b and 1d–1g). Two vast and naturally occurring oxygen minimum zones (OMZs) persist in the Arabian Sea and the Bay of Bengal, accounting for a disproportionately large fraction of the global volume of hypoxic waters (21%, Rixen et al., 2020). The rim of the northern Indian Ocean where the upper boundaries of the OMZs intersect the continental margins is subject to strong seasonal and interannual variations in coastal upwelling (Helly & Levin, 2004; Suresh et al., 2016, 2018), which can sustain or instigate coastal hypoxia by modulating the supply of oxygen-poor and nutrient-rich waters from the OMZs onto the continental shelf (e.g., Fennel & Testa, 2019; Garrison et al., 2000; Gupta et al., 2016; Levin et al., 2009; S. Naqvi et al., 2000; Sarkar et al., 2020; Sudheesh et al., 2016; Vallivattathillam et al., 2017). These nutrient-rich waters fuel primary production (e.g., Currie et al., 2013; Koné et al., 2009; Naqvi et al., 1979; Naqvi et al., 2006; Wiggett et al., 2005, 2009), promoting subsurface biological oxygen demand through respiration of sinking organic matter and potentially act as an amplifying biological feedback on hypoxia. Anthropogenic factors can also instigate or modulate coastal hypoxia. Observations suggest that warming-driven oxygen loss only had a mild effect in the northern Indian Ocean in the past decades (Banse et al., 2014; Piontkovski & Al-Oufi, 2015; Rixen et al., 2020), but coastal eutrophication could contribute significantly in the region. The countries that border the Indian Ocean account for about 30% of the world's population, with urbanization, untreated waste waters, and fertilizers leading to high inputs of nutrients into coastal waters (e.g., George et al., 2013; Martin et al., 2008; Naqvi et al., 2009; Seitzinger et al., 2010), which could further stimulate subsurface biological oxygen demand (Diaz & Rosenberg, 2008; Nixon, 1995; Rabalais et al., 2010). In this study, we focus on the impacts of the *natural* processes that contribute to coastal hypoxia on seasonal and interannual timescales in the northern Indian Ocean.

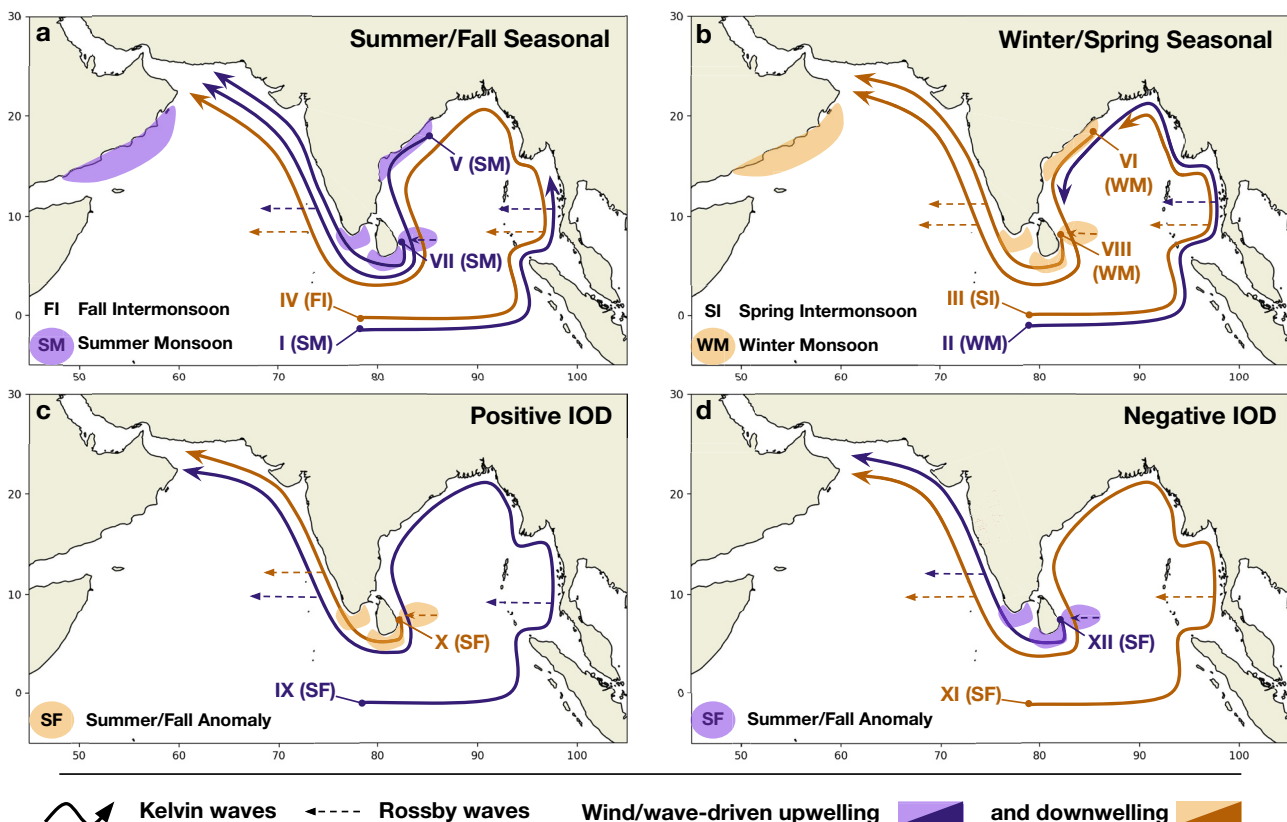


Figure 2. Schematic of the main processes associated with coastal (a and b) seasonal upwelling and downwelling, and (c and d) interannual upwelling and downwelling anomalies tied to the Indian Ocean Dipole phases. Shaded areas indicate wind-driven motions, solid arrows indicate Kelvin waves and dashed arrows indicate Rossby waves. Kelvin waves are labeled with roman numerals (I to XI) for reference in the text and in Figure 5. The season during which they are generated is indicated in parenthesis (SM and WM: Summer and Winter Monsoons, SI and FI: Spring and Fall Intermonsoons, SF: Summer/Fall).

Seasonal upwelling and downwelling motions in the coastal Indian Ocean are largely attributed to local winds or remotely forced coastal Kelvin waves tied to the Asian monsoon (e.g., McCreary et al., 1993; Nienhaus et al., 2012; R. Rao et al., 2010; Suresh et al., 2016; Vinayachandran et al., 2021; Yang et al., 1998). Locally, alongshore winds in the western Arabian Sea (WAS) and western Bay of Bengal are upwelling favorable during the summer monsoon (June–September, purple shaded regions Figure 2a), and downwelling favorable during the winter monsoon (December–April, orange shaded regions Figure 2b). The Arabian Sea and Bay of Bengal are also strongly influenced by a seasonal succession of upwelling and downwelling Kelvin waves originating from the Equator, the northwestern Bay of Bengal, and near the tip of India/Sri Lanka. These Kelvin waves are signal carriers, and efficiently transmit energy away from wind-forced areas. At the Equator, changes in zonal winds excite *upwelling* equatorial Kelvin waves during the summer and winter monsoons (purple arrows I and II), and *downwelling* equatorial Kelvin waves during the spring and fall monsoon transitions (orange arrows III and IV on Figures 2a and 2b). These four wave trains travel east, impinge on the coast of Sumatra, and continue counter-clockwise around the Bay of Bengal as *coastal* Kelvin waves, where they are modified by local winds (McCreary et al., 1996; Nienhaus et al., 2012; Suresh et al., 2016). The winter upwelling (II) and fall downwelling (IV) Kelvin waves extend farthest into the Bay of Bengal, with the fall downwelling wave reaching the eastern Arabian Sea (Nienhaus et al., 2012). In the northwestern Bay of Bengal, wind-driven summer upwelling and winter downwelling excite Kelvin waves of the same polarity that propagate equatorward along the western Bay of Bengal (arrows V and VI in Figures 2a and 2b), bend around Sri Lanka, and continue up the west coast of India. Finally, to the east of Sri Lanka, Rossby waves generated from interior wind stress curl travel west, and set up poleward traveling coastal Kelvin waves that are reinforced by alongshore wind stress near the tip of India/Sri Lanka region. These coastal Kelvin waves are upwelling waves in summer and downwelling waves in winter

(arrows VII and VIII in Figures 2a and 2b), and contribute to the majority of seasonal sea level variability along the west coast of India (Suresh et al., 2016).

Seasonal upwelling and downwelling are modulated from year-to-year by the main natural mode of climate variability affecting northern Indian Ocean sea level, the Indian Ocean Dipole (IOD) (Aparna et al., 2012; Currie et al., 2013; S. A. Rao & Behera, 2005; Suresh et al., 2018; Yu et al., 2005), which could influence the incidence, severity, or longevity of coastal hypoxia (e.g., Gupta et al., 2016; Lumban-Gaol et al., 2021; S. Naqvi et al., 2009; Nigam et al., 2018; Vallivattathillam et al., 2017). The IOD is one of the main sources of interannual anomalies in zonal wind and sea-surface temperature in the equatorial Indian Ocean (Saji et al., 1999; Webster et al., 1999). Positive IOD phases trigger upwelling Kelvin waves in the equatorial Indian Ocean in summer/fall that propagate counter-clockwise along the rim of the Bay of Bengal (purple arrow IX in Figure 2, Aparna et al., 2012; Han & Webster, 2002; R. Rao et al., 2010; Suresh et al., 2018). Meanwhile, in summer/fall downwelling Kelvin waves generated from both alongshore and interior wind stress near the tip of India and Sri Lanka propagate to the eastern Arabian Sea, and are followed in winter/spring by an upwelling Kelvin wave from the Bay of Bengal (Suresh et al., 2018, orange arrow X, purple arrow IX in Figure 2c). Similarly, negative IODs are associated with a downwelling coastal Kelvin wave in the Bay of Bengal and a succession of upwelling-downwelling Kelvin waves from summer/fall to winter/spring in the Arabian Sea (orange and purple arrows XI and XII in Figure 2d). Notably, on both seasonal and interannual timescales, poleward traveling Kelvin waves along the eastern coasts of the Arabian Sea and Bay of Bengal, as well as interior Ekman pumping, radiate Rossby waves that travel westward. These Rossby waves can extend the coastal signature of upwelling and downwelling by carrying the wind- and Kelvin wave-driven signals offshore along these eastern coasts (dashed arrows in Figure 2), and can also influence upwelling and downwelling along western coastlines (e.g., Suresh et al., 2016, 2018; Vic et al., 2017).

The seasonal and interannual processes controlling coastal upwelling, downwelling, and primary production are well documented in the northern Indian Ocean (e.g., Aparna et al., 2012; Clarke & Liu, 1994; Currie et al., 2013; Han & Webster, 2002; Lévy et al., 2007; R. Rao et al., 2010; S. A. Rao et al., 2002; Suresh et al., 2016, 2018; Webster et al., 1999; Wiggert et al., 2005, 2009; Vallivattathillam et al., 2017), and their influence on coastal hypoxia has been identified locally. For instance, observations revealed that seasonal hypoxia is tightly linked to summer/fall upwelling in the southeastern Arabian Sea (Gupta et al., 2016, 2021; Naqvi et al., 2009). Results from an ocean biophysical model suggested that the downwelling wave associated with positive IOD phases in summer/fall could limit the occurrence of hypoxia in the eastern Arabian Sea (Vallivattathillam et al., 2017), and observations support the alleviation of hypoxia in this region during positive IOD phases (Gupta et al., 2016; Naqvi et al., 2009). Here, we propose to expand on these prior results and evaluate the risk of coastal hypoxia at the scale of the entire northern Indian Ocean. We utilize a merged data set of in-situ measurement platforms paired with satellite products to diagnose the regions at higher risk of coastal hypoxia, and examine how this risk relates to seasonal and interannual physical and biological drivers associated with the Asian monsoon and the IOD.

2. Material and Methods

2.1. Coastal Indian Ocean Regions and Seasons

Four regions, the WAS, the eastern Arabian Sea (EAS), the western Bay of Bengal (WBoB), and the eastern Bay of Bengal (EBoB), are examined in this study (Figure 1). The WAS borders Yemen, Oman, Iran, and western Pakistan. The EAS spans eastern Pakistan, the western coast of India, and the southeastern coast of Sri Lanka. The WBoB borders the northeastern coast of Sri Lanka, and the east coast of India. Finally, the EBoB spans the northeastern coast of India, Bangladesh, Burma, Thailand, Malaysia, and Indonesia. These regions coincide with reported cases of coastal hypoxia (Breitburg et al., 2018), and have relatively consistent seasonal and interannual sea level anomaly signals throughout each region (e.g., upwelling in summer throughout EAS, Figures S1–S3 in Supporting Information S1). We define our coastal domain based on the extent of the coastal wave guides in the northern Indian Ocean from theory (Shetye, 1998, see their Figure 6) as well as from our sea level observations (Figures S1–S4 in Supporting Information S1). In the EAS and EBoB, where the continental shelf is wider and Rossby waves carry coastal Kelvin wave signals further offshore (Shetye, 1998; Suresh et al., 2016, 2018). In these two regions, we therefore use an extended coastal domain in which the outer limit of the mask is either approximately 300 km distance from the coast or the 1,000 m isobath, whichever is further

(Laruelle et al., 2017), and we have excluded profiles surrounding the Andaman and Nicobar Islands. In the WAS and WBoB, where the continental shelf is narrower and Rossby waves are not radiated from the coast, we use a narrower domain that extends approximately 150 km from the coast (NASA Ocean Biology Processing Group (OBPG) & Stumpf, 2012). Within each region, we grouped observations into two seasons: summer/fall (June–November) and winter/spring (December–May).

2.2. Observed Profiles

Oxygen, temperature, salinity, nitrate, and phosphate profiles from the World Ocean Database 2018 (WOD, Boyer et al., 2018) and its quarterly updates through 31 May 2020 were extracted with expendable bathythermograph corrections applied following Levitus et al. (2009), and only accepted profiles based on World Ocean Database flags were used from 1958 through 2020 (Figure 1). We use a threshold of 61 µmol/kg to define hypoxic waters following the definition used in Breitburg et al. (2018), and identify waters with oxygen levels between 61 and 80 µmol/kg as “vulnerable” to hypoxia. Most of the oxygen observations used in this analysis were made on or after 1960 (Figure 1c) to limit poor-quality measurements. Note that this is line with the World Ocean Atlas 2018 oxygen climatology protocol which also excluded measurements prior to 1960 (Garcia et al., 2019). Measurements from the earliest decades may still be biased high at low levels of oxygen (Bianchi et al., 2012). However, we expect this bias to influence long-term trend estimates rather than the seasonal or interannual results presented here. The potential effects could be an under-estimation of the degree of hypoxia in our study, and our results should be taken as a lower bound on the risks of hypoxia. In our analysis all profiles were averaged from 50 to 200 m, a depth range representative of typical shelf waters that also captures the average oxycline for all regions (Figure 1). We note that our results were only mildly sensitive to the lower and upper limits of this choice, with little changes for 50–225 and 40–200 m averages (Figures S5 and S6 in Supporting Information S1).

2.3. Satellite Products

Daily sea level anomalies (SLA) spanning January 1993 to May 2020 were used to isolate wave propagation as well as wind- and wave-driven upwelling. The daily sea-level anomaly data was linearly detrended in time (with intercept) at each spatial location to remove the effects of sea level changes associated with upper-ocean temperature trends (Thompson et al., 2016). Monthly surface chlorophyll-a spanning September 1997 to May 2020 (Sathyendranath et al., 2019) was used to assess the potential for biological feedbacks associated with upwelling and downwelling (e.g., the supply of low oxygenated waters could be reinforced by increased surface biological production and subsurface oxygen demand). Monthly climatologies for both datasets were calculated by first averaging daily data to monthly if needed, then averaging all data for a given month over the observed period. Interannual anomalies were found by subtracting the monthly climatology from the observed monthly signal.

2.4. Dipole Mode Index and IOD Phases

For our analysis, interannual SLA and 50–200 m oxygen values during positive, negative, and neutral IOD phases were grouped and averaged together beginning in June 1st of a given IOD year through May 31st of the following year. IOD phases were identified using the Dipole Mode Index (DMI). A DMI time series from 1958 to 1999 (Saji et al., 1999) was merged with a more recent time series spanning from 1981 to 2020 that was resampled to monthly time intervals. The 1958–1999 time series was scaled by the ratio of the 1981–2020 data set's standard deviation to its own, and the average of both datasets was taken for the overlapping years from 1981 to 1999. A centered 3-month running mean was applied to the merged time series (Figure S7 in Supporting Information S1). Positive (negative) IOD years correspond to years where the September–October–November average is larger (less) than 1 (-1) standard deviation of the data. Within ± 1 standard deviation, the year was considered neutral. If it was greater than 2 standard deviations it was classified as a strong positive IOD year. The DMI is not the only index available to diagnose IOD phases, but at least for the 1993–2018 period, it is very similar to the sea level dipole index, wind stress dipole index, or the outgoing longwave radiation based index (Akhil et al., 2020, see their Figure 3). The exceptions are during 2017 and 2018 when the DMI is larger than the other indices. However, 2017 was not detected as an IOD event, and 2018 was detected as a relatively weak IOD event by our methodology (Figure S7 in Supporting Information S1) and has therefore a marginal impact on our results.

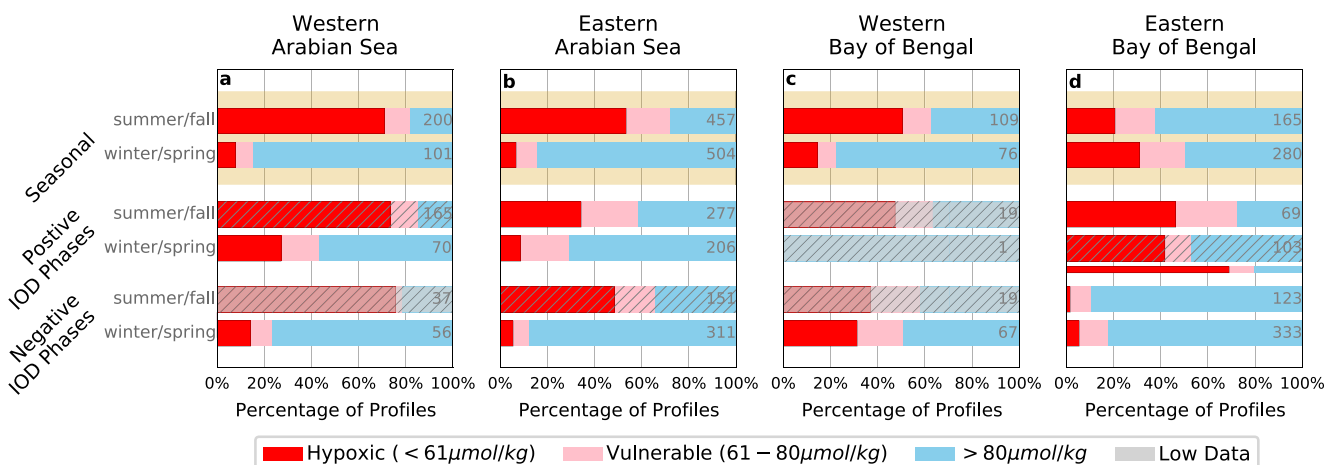


Figure 3. Percentages of World Ocean Database profiles with shelf oxygen levels (50–200 m average) that were hypoxic ($< 61 \mu\text{mol/kg}$) or vulnerable ($61–80 \mu\text{mol/kg}$) for the (a) western Arabian Sea (WAS), (b) eastern Arabian Sea (EAS), (c) western Bay of Bengal (WBoB), and (d) eastern Bay of Bengal (EBBoB). For each region, seasonal (top row of bars), positive Indian Ocean Dipole (IOD, middle row of bars), and negative IOD (bottom row of bars) percentages are shown for summer/fall and winter/spring. Strong positive IOD percentages are plotted as a thin bar for winter/spring (below the all positive IOD phase) in the EBBoB. Seasonal percentages are evaluated using neutral IOD years. The number of available observations is indicated in gray (58 observations for EBBoB strong positive IOD). Shading masks bars with less than 40 observations and hatching indicates when IOD cumulative distribution functions were not distinct from neutral phases (95% confidence limit, Figures S7 and S8 in Supporting Information S1). Profile locations and the observation distribution by month are given in Figure S10 of Supporting Information S1.

2.5. Statistics

Cumulative distribution functions (CDFs, Figures S8 and S9 in Supporting Information S1) were estimated by dividing the number of observations below or at an observed oxygen value by the total number of oxygen observations, then converting to percentage. The CDFs were compared to determine if positive and negative IOD CDFs were distinct from neutral IOD CDFs (taken as a proxy for seasonal CDFs), or if strong positive IOD CDFs were distinct from the CDFs for all positive IOD phases. Distinctions were identified with the Kolmogorov-Smirnov test (Young, 1977), which was implemented with `ks_2samp` function. A large Kolmogorov-Smirnov statistic indicates larger deviations between the compared CDFs. The p -value associated with the Kolmogorov-Smirnov statistic corresponds to a two-sided test under the null hypothesis that the two independent samples are drawn from the same continuous distribution. To determine the correlation coefficients and linear regressions of Figure 4 and Figure S11 in Supporting Information S1, SLA was linearly interpolated to the latitude and longitude of all WOD profiles. To determine the correlations in Figure 6, chlorophyll-a was linearly interpolated to SLA locations. The interpolations for all datasets were found using the `griddata` function. All linear regressions, correlation coefficients, and p -values were found with the `linregress` function. The functions `ks_2samp`, `griddata`, and `linregress` are from SciPy v1.3.0 (Virtanen et al., 2020).

3. Results

3.1. Drivers and Timing of Seasonal Hypoxia

Coastal hypoxia is highly prevalent throughout the entire northern Indian Ocean, with observations of oxygen on the shelf (defined as 50–200 m average within the coastal domain) that fall below the hypoxic level in each of the four regions analyzed here (eastern/western AS, eastern/western BoB, Figure 1b). The occurrence of hypoxia is quantified in Figure 3, which shows the percentage of profiles in the database where oxygen values on the shelf are hypoxic ($< 61 \mu\text{mol/kg}$), vulnerable ($61–80 \mu\text{mol/kg}$), or greater than $80 \mu\text{mol/kg}$ during summer/fall and winter/spring for each region. We evaluate the seasonal risk of hypoxia using observations during neutral IOD phases (i.e., excluding observations during positive and negative IOD phases, see Methods section). The risk of coastal hypoxia is highest in summer/fall in three of the four regions. The percentage of hypoxic profiles increases by 3–8 fold from winter/spring to summer/fall in the western AS (from 8% to 71%), the eastern AS (from 7% to 53%), and the western BoB (from 14% to 50%, Figures 3a–3c). In contrast, seasonal monsoons have an opposed but weaker impact in the eastern BoB, where the occurrence of hypoxia slightly increases from summer/fall to winter/spring (from 21% to 31%, Figure 3d). Vulnerable profiles ($61–80 \mu\text{mol/kg}$), account for

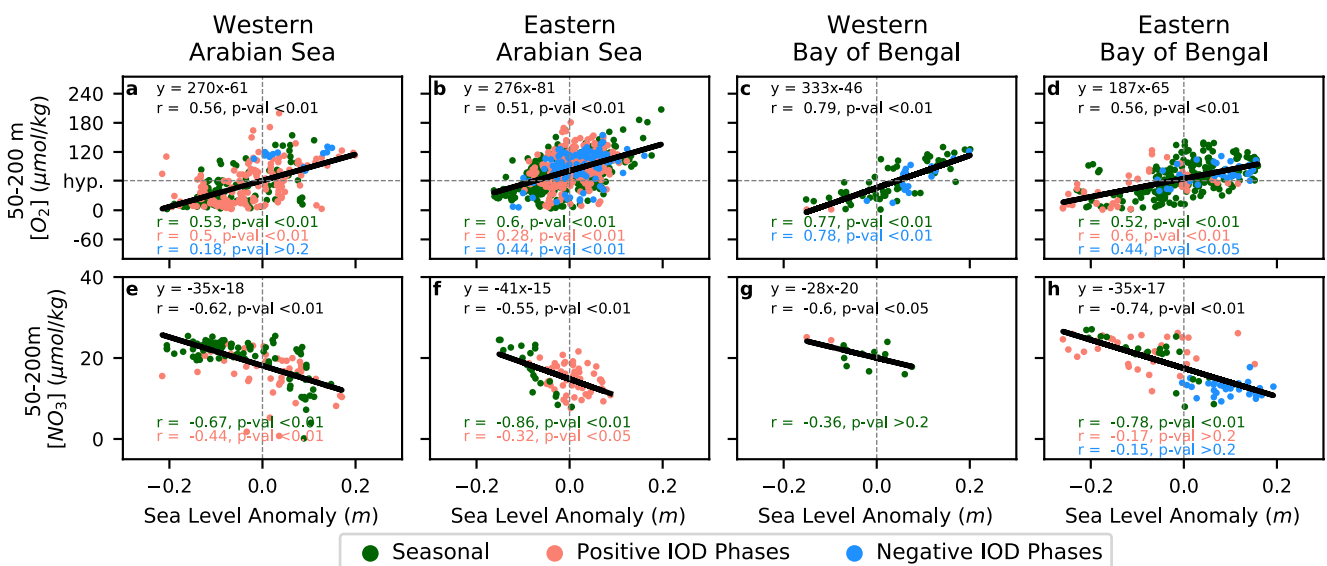


Figure 4. Correlations between sea level anomalies and 50–200 m dissolved oxygen (a–d) and nitrate (e–h) for the western Arabian Sea (WAS), eastern Arabian Sea (EAS), western Bay of Bengal (WBoB), and eastern Bay of Bengal (EBoB). A positive correlation indicates that upwelling (negative SLA) corresponds to a decrease in the average property (e.g., oxygen) from 50 to 200 m, and vice versa for positive SLA/negative correlations. The linear fit, Pearson correlation coefficient (r) and p -values (p -val) are given for the total data set within each region in black. Seasonal (i.e., neutral), positive, and negative IOD phase oxygen values are indicated by different colors, as are their corresponding correlation coefficients and p -values. Significance thresholds ($\alpha = 0.01, 0.05, 0.1$, and 0.2) are provided for the p -values, which correspond to rejection of the null hypothesis that the slope is zero at the $(1-\alpha)\%$ significance level. Horizontal gray dashed line in the first row indicates a hypoxic threshold of $61 \mu\text{mol}/\text{kg}$. Note that the correlations are only available after 1993 when SLA data was present. Correlations for temperature and phosphate are given in S11, and locations of the data used in the oxygen-SLA correlations are given in Figure S12 of Supporting Information S1.

about 10–20% of profiles in all regions and seasons, with highest occurrence in the eastern AS during summer/fall (19%, Figure 3b) and in the eastern BoB year round (17%–19%, Figure 3d).

We find that seasonal upwelling and downwelling are a prevalent source of oxygen variations within the coastal Indian Ocean. In all four coastal regions, upwelling conducive sea-level anomalies (negative SLA) are associated with decreased 50–200 m temperature and oxygen levels and increased nutrient concentrations, highlighting the role of ocean circulation in supplying cold, oxygen-poor and nutrient-rich OMZ waters to the shelf (Figure 4 and Figure S11 in Supporting Information S1). Likewise, downwelling conducive SLA (positive SLA) are associated with increased 50–200 m temperature and oxygen values but reduced nutrient concentrations, indicating that downwelling limits the supply of OMZ waters to the shelf (Figure 4). The key role of seasonal upwelling/downwelling is further supported by Figure 5 which shows the distribution of upwelling (purple contours) and downwelling (orange contours) inferred from SLA along the equatorial and coastal wave guides. Coastal SLA captures upwelling and downwelling motions, which are largely controlled by local wind (non-propagating signals such as in the western AS) and by Kelvin waves that propagate from the equator or tip of India along the coastal wave guides (counter-clockwise propagating signals such as in the Bay of Bengal and Arabian Sea, Figure 5).

Seasonal upwelling and downwelling motions have a similar timing in the western AS, western BoB and eastern AS during summer/fall. During the summer monsoon and fall inter-monsoon, wind-driven upwelling in the western AS and western BoB as well as wave-driven upwelling in the eastern AS (purple shading and waves V/VII in Figures 2a and 5a) are consistent with the higher percentage of hypoxic profiles observed in summer/fall in these three regions (Figures 3a–3c). In comparison, the winter monsoon and spring inter-monsoon are characterized by downwelling (orange shading and waves VI/VIII in Figures 2b and 5a), also consistent with the fewer hypoxic profiles found in winter/spring (Figures 3a–3c). We note that in the western BoB, the winter wind-driven downwelling competes with the propagation of a decaying wave-driven upwelling in spring (wave II in Figures 2b and 5a). Our results suggest that the influence of the winter wind-driven downwelling exceeds the effect of the decaying spring upwelling wave in controlling hypoxia in winter/spring (i.e., the occurrence of hypoxia is weaker in winter/spring than in summer/fall). The timing of upwelling/downwelling and the amplitude of the oxygen response in the eastern BoB contrast from the three other regions. In winter/spring, wave-driven

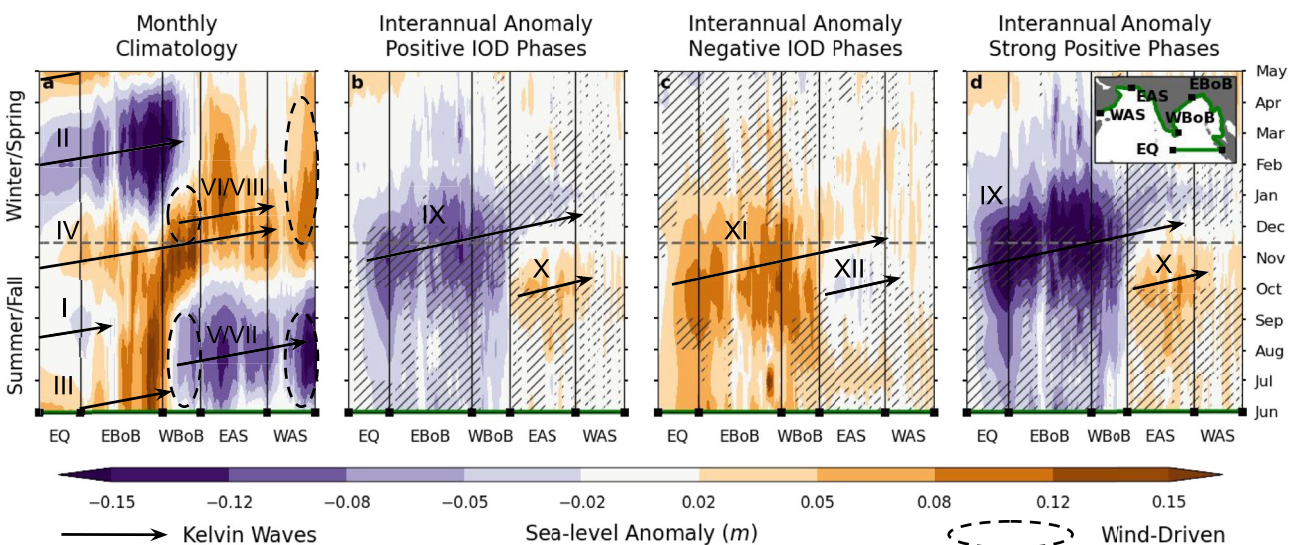


Figure 5. Coastal upwelling/downwelling associated with local winds and Kelvin wave propagation in the northern Indian Ocean inferred from sea level anomalies (SLA). (a) Seasonal cycle of coastal SLA (1993–2020 data average). (b and c) Interannual SLA (seasonal cycle removed) for (b) positive Indian Ocean Dipole (IOD) phases (1994, 1997, 2006, 2012, 2015, 2018, 2019), (c) negative IOD phases (1996, 1998, 2010, 2016), and (d) strong positive IOD phases only (1994, 1997, 2006, 2019). Upwelling is indicated by negative sea level anomalies and downwelling is indicated by positive sea level anomalies. Wind-driven upwelling/downwelling regions are circled and coastal Kelvin waves are indicated by arrows and the roman numerals used in Figure 2. The arrows indicate an approximate wave speed of 2.4 m/s, which is on par with theoretical estimates for first baroclinic mode Kelvin waves. The x-axis follows the equatorial and coastal wave guides (green line in inset d) starting at the equator (EQ), counterclockwise around the Bay of Bengal (E/WBoB), around Sri Lanka and the tip of India, and counterclockwise around the Arabian Sea (E/WAS). Unhatched regions indicate where the IOD anomaly reinforces the seasonal signal, while hatching indicates where IOD and seasonal signals oppose each other. The horizontal dashed line delimits winter/spring and summer/fall. Months start in June of an IOD year and end in May of the following year.

upwelling reinforced by local winds (wave II in Figures 2b and 5a) yields a modest increase in hypoxic profiles compared to summer/fall, when downwelling prevails (Figure 3d).

While the total number of observations per region on seasonal timescales is relatively large, there are sampling issues that could influence the percentages shown in Figure 3. For instance, the seasonal contrast in coastal hypoxia is weaker in the eastern BoB than in the other three regions (21%–31% hypoxic profiles between summer/fall and winter/spring Figure 3) despite similar upwelling/downwelling intensities (Figure 5a). This is consistent with the mean profiles in this region which show little differences between seasonal oxyclines (Figure 1g). A possible cause is the sampling distribution within the eastern BoB. In summer/fall, sampling is split between northeastern BoB downwelling and southeastern BoB neutral to weak upwelling (Figure S10 in Supporting Information S1), which could explain the muted effects of downwelling in the seasonal and regional average (Figure 3d). Finally, we show that weaker reinforcing biological feedbacks might also explain part of the eastern BoB muted response (see the Biological Feedback section). Another potential bias could come from the larger proportion of observations during summer (June–September) upwelling than fall (October–November) downwelling in the western BoB (Figure S10 in Supporting Information S1), which could bias high the percentage of hypoxic profiles when combining summer and fall. Finally, Kelvin wave-driven upwelling motions on the western sides of basins could be more coastally confined than wind-driven upwelling (Figure S1 in Supporting Information S1). As a result, the database may undersample the wave driven signal compared to the wind driven signal, potentially biasing the percentages of hypoxic profiles low in the western BoB during winter/spring when both wind-driven downwelling and wave-driven upwelling are present (dashed oval and II in Figure 5a respectively).

3.2. Influence of the Indian Ocean Dipole on Coastal Oxygen Levels

To evaluate the influence of year-to-year IOD variations on seasonal hypoxia, we compare the percentage of hypoxic profiles during positive and negative IOD phases to the seasonal percentages observed during neutral phases (Figure 3). The eastern BoB is the only region that is substantially influenced by both positive and negative IOD phases (Figure 3d). In this region, positive IODs favor the occurrence of hypoxia year-round, with the

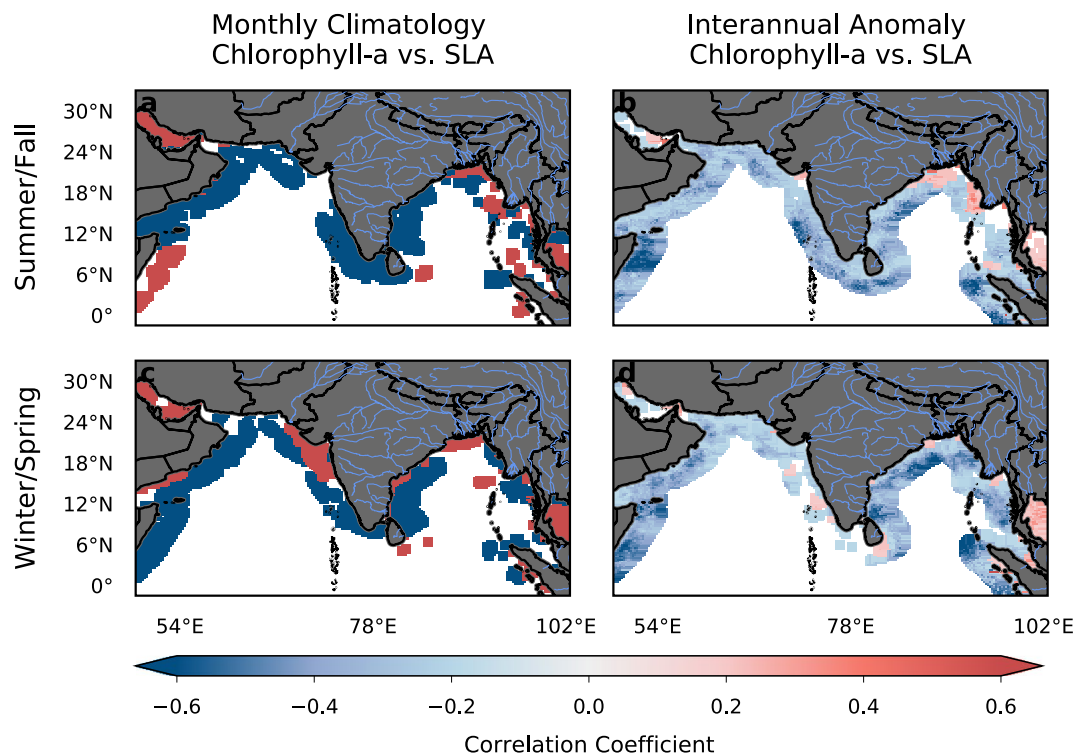


Figure 6. (a and c) Correlation between the mean annual cycle calculated with data from 1997 to 2020 of chlorophyll-a and sea-level anomalies (SLA), and (b and d) *interannual* chlorophyll-a anomalies correlated with *interannual* sea-level anomalies. A negative correlation indicates that upwelling (negative SLA) corresponds to an increase in surface chlorophyll, and vice versa for positive SLA/positive correlations. Correlations that were not significant at the 95% confidence limit, or further than approximately 300 km from the coast were not plotted.

fraction of hypoxic observations increasing by 25% in summer/fall compared to neutral years, pushing the risk of hypoxia above 40%. In contrast, negative IOD phases reduce the fraction of hypoxic profiles by 19% in summer/fall and by 26% in winter/spring, suppressing almost entirely the risk of hypoxia. The coasts of the AS are mostly influenced by positive IODs, which reduce the risk of hypoxia from 53% to 34% in the eastern AS during summer/fall, and increase the risk of hypoxia from 8% to 27% in the western AS during winter/spring (Figures 3a and 3b). In contrast, we find little influence of negative IOD phases in the AS (Figures 3a and 3b). In the western BoB, the data coverage is insufficient to evaluate the impact of IOD except during negative IOD phases in winter/spring where the prevalence of hypoxia is increased from 14% to 31% (Figure 3c).

As on seasonal timescales, interannual changes in the occurrence of hypoxia can be tied to upwelling/downwelling motions that modulate the supply of oxygen-poor OMZ waters onto the shelf (Figure 4). We examine interannual SLA signals associated with positive and negative IOD phases. In the BoB, positive IODs are associated with a strong anomalous upwelling Kelvin wave and negative IODs with a strong anomalous downwelling Kelvin wave (waves IX and XI in Figures 2c, 2d, 5b, and 5c). Both anomalous Kelvin waves propagate along the eastern BoB in summer/fall and persist into winter/spring, which explains the substantial year-round increase (decrease) in hypoxia during positive (negative) IODs in this region (Figure 3d). We note that the upwelling/downwelling anomaly signals typically peak in fall and winter during IOD phases (Figures 5b and 5c), and the effects on hypoxia are likely strongest during these periods in the eastern BoB. In contrast, the increased winter/spring risk of hypoxia during negative IODs in the western BoB (Figure 3c) is inconsistent with the downwelling anomaly in this region (Figure 5b). As on seasonal timescales, sampling issues may explain this discrepancy. Most of the data in this region is in January, when the anomalous downwelling signal is decaying, and April, when it has nearly vanished but seasonal upwelling is prevalent (Figures 5a and 5c, Figure S10 in Supporting Information S1), thus biasing the percentage of hypoxic profiles high.

In the AS, positive and negative IOD phases are associated with downwelling and upwelling Kelvin waves, but we focus here on positive IODs because they are the main source of variability in hypoxia in this region (Figures 3a and 3d). Positive IODs are characterized by downwelling Kelvin waves generated near the tip of India that propagate along the west coast of India during summer/fall, followed by an upwelling Kelvin wave originating in the BoB in winter/spring (waves X and IX in Figures 2c and 5b). The downwelling Kelvin wave opposes seasonal upwelling in early fall, while the upwelling Kelvin wave opposes seasonal downwelling in winter/spring (hatched regions in Figure 5b). In the eastern AS, this succession of summer/fall downwelling and winter/spring upwelling is consistent with the lesser number of hypoxic profiles observed in summer/fall and the larger number of vulnerable profiles observed in winter/spring during positive IODs (Figure 3b). These IOD-driven downwelling/upwelling motions have minor influence in the western AS, likely due to the dominance of seasonal wind-driven variability (Figure 5a dashed ovals and SLA poorly correlated with the DMI in this region, Figure S4 in Supporting Information S1), the decay of the Kelvin wave signals by the time they reach this area (Figures 5b and 5c), and the presence of gaps (e.g., Persian Gulf) in the coastal wave guide. The very weak upwelling anomaly in winter/spring of positive IODs is nevertheless consistent with the 19% increase in hypoxia observed in the western AS (Figures 3a and 5b).

3.3. Extreme Positive Indian Ocean Dipole Events

Strong positive IODs increase the risk of hypoxia in the eastern BoB in winter/spring. The threat of hypoxia is 27% greater during the strong positive IODs sampled by the World Ocean Database (1961, 1972, 1994) than that considering all positive IODs, and 38% greater than the seasonal risk (see small horizontal bar in Figure 3d). During strong positive IODs within the SLA record (1994, 1997, 2006, 2019) the upwelling Kelvin wave that begins in June at the equator and transits through the BoB from October through January is stronger than that for the average of all positive IODs by up to 0.10 m (wave IX in Figure 5d), consistent with more instances of hypoxia in the eastern BoB during strong positive IODs (Figure 3d, thin bar).

SLA is larger by as much as 0.10 m year-round in the western BoB, indicating stronger upwelling. Additionally, the succession of summer/fall downwelling and winter/spring upwelling Kelvin waves are reinforced by as much as 0.05 m in the eastern AS (Figure 5d). Oxygen observations are, however, insufficient to evaluate the impact of these extreme cases on coastal hypoxia in the western BoB, and differences in the occurrence of hypoxia between all positive IODs and for strong positive IODs are not significant for the entire AS (Figure S9 in Supporting Information S1).

3.4. Biological Feedbacks

Figure 4 shows that, in addition to oxygen-deficient waters, seasonal and interannual upwelling brings nutrient-rich waters onto the shelf, as upwelling conducive SLA generally coincides with increased subsurface nitrate concentrations in all regions for all seasons and during all IOD phases (we find a similar result for phosphate, see Figure S11 in Supporting Information S1). The enhanced subsurface biological oxygen demand could reinforce low-oxygen levels from upwelled OMZ waters, sustaining or increasing the intensity of existing coastal hypoxia. The impact these nutrients actually have on coastal hypoxia is, however, difficult to quantify from these correlations alone. Here, we evaluate regions where this re-inforcing biological or “respiration” feedback might be at play on seasonal and interannual timescales using surface chlorophyll-a as an indicator of subsurface oxygen demand, as well as how it correlates to SLA, which we take as a proxy for upwelling/downwelling motions (Figure 6). Locations where this positive feedback exists are expected to have a negative correlation, where upwelling (negative SLA) corresponds to increased chlorophyll, or downwelling (positive SLA) corresponds to decreased surface production.

Seasonally, we find that the risk of hypoxia from biological processes likely compounds the risk from physical upwelling in the AS and western BoB in summer/fall, where upwelling is associated with enhanced chlorophyll-a (negative correlation between SLA and chlorophyll-a, blue in Figures 6a and 6c). In the eastern BoB, however, the correlation is not significant, suggesting a weaker biological feedback that could partially explain the weak seasonal contrast found in the occurrence of hypoxia in this region (Figure 3). We note that there are pockets in the northeastern AS and BoB where SLA is positively correlated with chlorophyll-a (i.e., reduced chlorophyll-a during upwelling phases, red in Figures 6a and 6c). Most of these regions coincide with river outflows,

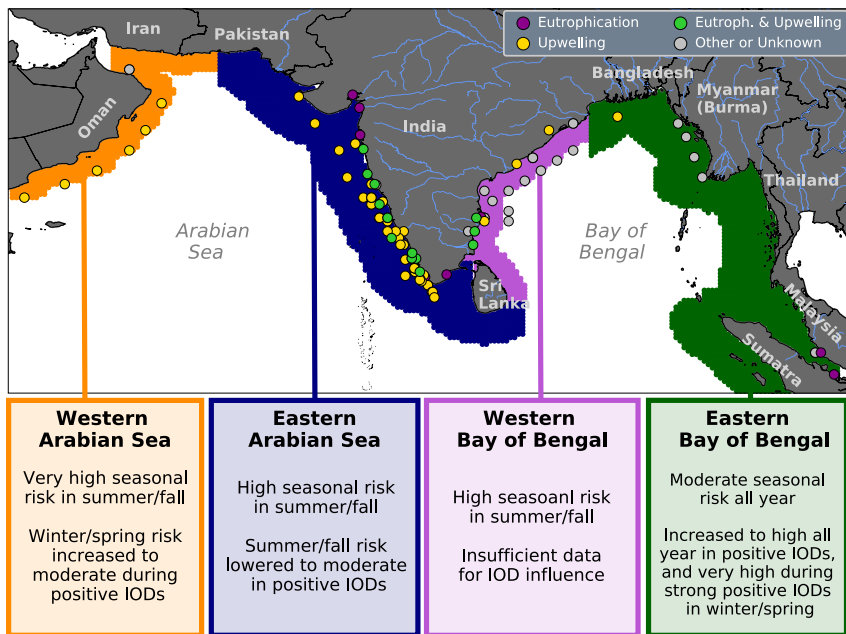


Figure 7. Risk of coastal hypoxia tied to seasonal monsoons and the interannual Indian Ocean Dipole in the four regions analyzed in this study. Risk levels are determined using the percentages from Figure 3. Very high risk is >60%, high risk is 40%–60%, moderate risk is 20%–40%, and low risk is <20%. Reported cases of hypoxia from Breitburg et al. (2018) and our updates are plotted based on the driving factors (see legend, supporting data set). The colors of markers indicate the associated drivers of hypoxia per the literature. This includes eutrophication, upwelling, both, or other or unknown. Here “other” includes mechanisms such as tropical cyclones and eddies, and “unknown” means the driver was not identified in the publication.

where chlorophyll-a and production are likely controlled by riverine nutrient loadings and estuarine dynamics (for instance stronger stratification may limit production, Prasanna Kumar et al., 2002). In addition, large seasonal changes in river inputs of terrestrial material might bias satellite retrievals of chlorophyll-a (Poddar et al., 2019), thus obscuring the link between upwelling/downwelling and chlorophyll-a in these regions.

On interannual timescales, upwelling is also linked to increased production almost everywhere in the northern coastal Indian Ocean, although the correlations are generally weaker than on seasonal timescales (Figure 6). In the eastern AS, however the correlation is not significant in winter/spring (Figure 6d). The succession of upwelling and downwelling waves during winter/spring in this region (Figures 5b and 5c) could lead to a mixed signal in chlorophyll-a, and hence a lack of correlation in this region. While these results are significant, we reiterate that our approach to assess this feedback is qualitative, and describe possible future refinements in Section 4 that follows.

4. Summary and Discussion

The northern Indian Ocean is subject to strong upwelling and downwelling, modulated seasonally by the Asian monsoon and interannually by the IOD. This work quantifies the seasonal and interannual risk of hypoxia associated with these upwelling/downwelling motions and the potential reinforcing biological respiration feedback—whereby upwelling/downwelling lead to increased/decreased subsurface oxygen demand—for the coastal northern Indian Ocean. A schematic of our main results is presented in Figure 7. Seasonally, the risk of hypoxia is highest in the entire AS and western BoB (i.e., Oman, Iran, Pakistan, India, Sri Lanka) in summer/fall due to a combination of wind- and wave-driven upwelling, as well as potentially an increase in biological oxygen demand. This is consistent with prior reports of hypoxia linked to seasonal upwelling within the western AS (Piontkovski & Al-Oufi, 2015), the eastern AS (Banse, 1959; Carruthers et al., 1959; Gireeshkumar et al., 2017; Gupta et al., 2016, 2021; Jaleel et al., 2014, 2015, 2021; Martin et al., 2010; S. Naqvi et al., 2000, 2006; Padma-kumar et al., 2016; Parameswaran et al., 2018; Shirodkar et al., 2018), and the western BoB (S. Naqvi et al., 1979; Satpathy et al., 2013). We note that there are more historically reported cases of seasonal hypoxia in the eastern

AS and western BoB than the other two regions analyzed in our study (Figure 7). This is likely due to better monitoring and reporting, as well as the intensity of the seasonal dead zone compared to the other regions (e.g., S. Naqvi et al., 2009).

On interannual timescales, the risk of hypoxia is modulated by IOD anomalies in upwelling and downwelling motions. In the eastern BoB (i.e., Bangladesh, Myanmar, Thailand, Malaysia, Sumatra) the risk is increased from moderate to high year-round during positive IODs, and decreased from moderate to low during negative IODs. We note that during strong positive IOD phases, the risk is increased from moderate to very high in winter/spring. The strength and frequency of positive IOD events have increased over the latter half of the 20th century (Abram et al., 2008), including an unusual number of strong positive IOD events since 1960 compared to the last millennium (Abram, Wright, et al., 2020). The frequency of extreme positive events is projected to increase under climate change (Abram, Hargreaves, et al., 2020; Cai et al., 2021), suggesting that the eastern BoB could be particularly vulnerable to hypoxia in the future. Finally, in the eastern AS (i.e., west coast of India, southwestern Sri Lanka), the risk of summer/fall hypoxia is reduced from high to moderate during positive IOD phases. This is consistent with the modeling results of Vallivattathillam et al. (2017), who showed that positive IODs reduce the supply of low-oxygen waters to the shelf associated with the seasonal upwelling in a sub-region of the eastern AS, and is further supported by interannual observations of coastal oxygen that suggest hypoxia is less severe during positive IOD phases from less intense upwelling of oxygen-poor and nutrient-rich waters from the Arabian Sea OMZ (Gupta et al., 2016). Due to lack of long-term co-located measurements, as well as the sparsity of IOD events over the instrumental record, comparisons with historical reports of hypoxia in the other three regions could not be made.

We focused our analysis on the influence of upwelling and downwelling and a qualitative assessment of biological feedbacks because they explain, to first order, the occurrence of hypoxia in the northern Indian Ocean. The risk evaluation proposed here could be refined by analyzing the four seasons separately (Summer, Fall, Winter, Spring) instead of grouping them into two (Summer/Fall, Winter/Spring) as adequate data becomes available to do so, as well as better quantifying the influence of the *positive* biological respiration feedback and the influence of other potential *negative* biological feedbacks, such as the switch to nitrate-based respiration at low oxygen levels (denitrification, Lachkar et al., 2016; S. Naqvi et al., 2006). Our results suggest that the respiration feedback is present throughout the entire Indian Ocean, except near river mouths and in the EBoB on seasonal timescales. They also suggest that this feedback likely plays less of a role on interannual timescales (in particular in the eastern Arabian Sea). Yet, chlorophyll-a only provides qualitative information about changes in surface production and subsurface biological demand. Chlorophyll concentration in phytoplankton is influenced by light and iron availability, as well as phytoplankton species (e.g., Geider et al., 1997). Additionally, satellite based retrievals are biased by a number of factors including the presence of colored organic matter from terrestrial origin, cloud cover, heterogenous water columns, and by merging information from multiple sensors (e.g., Blondeau-Patissier et al., 2014; Poddar et al., 2019; Sathyendranath et al., 2019). Evaluating the magnitude of the biological feedback on coastal hypoxia would require a detailed oxygen budget (Fennel & Testa, 2019) of the coastal domain using either a biogeochemical model (e.g., Cui et al., 2019; Resplandy et al., 2012) or fine observations of ocean circulation and oxygen consumption and production (e.g., Brandt et al., 2015; Llanillo et al., 2018; Long et al., 2019).

Future risk evaluations should also include the impact of other factors, such as variations in rainfall or eutrophication (e.g., Fennel & Testa, 2019), which could introduce some decoupling between upwelling and the hypoxic response. For instance, in the northwestern Bay of Bengal (alongside sampling issues), riverine nutrient inputs could be important contributors to the increased risk of hypoxia in spite of downwelling conducive sea-level anomalies during negative IOD phases in winter/spring. Reported cases of eutrophication related hypoxia are already prevalent in the northern Indian Ocean (purple dots in Figure 7), and increased nutrient loading has been linked to intensification of upwelling-driven seasonal hypoxia along the coast of the southwestern Bay of Bengal (Satpathy et al., 2013) and eastern Arabian Sea (e.g., Martin et al., 2010; S. Naqvi et al., 2000; Padma-kumar et al., 2016) (green dots in Figure 7). Due to population growth (Samir & Lutz, 2017) and high dependency on crops and fertilizer use (Seitzinger et al., 2010; Sinha et al., 2017), eutrophication is likely to exert a stronger control on coastal hypoxia in the future. This could be particularly important for regions where seasonally the percentage of vulnerable profiles is comparable to the percentage of hypoxic profiles, such as the EBoB (Figure 3d). Future studies are thus needed to address the expanding role of human-driven hypoxia in combination with the risks posed by the natural factors highlighted here.

Data Availability Statement

All data used in this study is freely available online, with the exception of the hypoxia records and DMI data set included in Supporting Information S1. All profile data can be extracted from the World Ocean Database (<https://www.ncei.noaa.gov/products/world-ocean-database>). Daily sea-level anomalies (version vDT2018, 0.25° resolution) can be retrieved from the Copernicus Climate Data Store <https://cds.climate.copernicus.eu/cdsapp#!/dataset/satellite-sea-level-global>. Daily surface chlorophyll-a (version 5.0, nominal 4 km resolution) are available at the ESA Ocean Colour Change Climate Initiative website (<https://climate.esa.int/en/projects/ocean-colour/data/>). Computer code to process the raw data and produce the figures are publicly available at <https://github.com/jlpearso/coastlines-at-risk-of-hypoxia-in-the-northern-indian-ocean>.

Acknowledgments

This study has been supported by the National Science Foundation CAREER award 2042672, the Cooperative Institute for Modeling the Earth System between the National Oceanic and Atmospheric Administration Geophysical Fluid Dynamics Laboratory and Princeton University, the High Meadows Environmental Institute Carbon Mitigation Initiative and Grand Challenges programs, and the Sloan Foundation.

References

- Abram, N. J., Gagan, M. K., Cole, J. E., Hantoro, W. S., & Mudelsee, M. (2008). Recent intensification of tropical climate variability in the Indian Ocean. *Nature Geoscience*, 1(12), 849–853. <https://doi.org/10.1038/ngeo357>
- Abram, N. J., Hargreaves, J. A., Wright, N. M., Thirumalai, K., Ummenhofer, C. C., & England, M. H. (2020). Palaeoclimate perspectives on the Indian Ocean Dipole. *Quaternary Science Reviews*, 237, 106302. <https://doi.org/10.1016/j.quascirev.2020.106302>
- Abram, N. J., Wright, N. M., Ellis, B., Dixon, B. C., Wurtzel, J. B., England, M. H., et al. (2020). Coupling of Indo-Pacific climate variability over the last millennium. *Nature*, 579(7799), 385–392. <https://doi.org/10.1038/s41586-020-2084-4>
- Akhil, V. P., Vialard, J., Lengaigne, M., Keerthi, M. G., Boutin, J., Vergely, J.-L., & Papa, F. (2020). Bay of Bengal sea surface salinity variability using a decade of improved SMOS re-processing. *Remote Sensing of Environment*, 248, 111964. <https://doi.org/10.1016/j.rse.2020.111964>
- Aparna, S., McCreary, J., Shankar, D., & Vinayachandran, P. (2012). Signatures of Indian Ocean Dipole and El Niño–Southern Oscillation events in sea level variations in the Bay of Bengal. *Journal of Geophysical Research*, 117(C10), C10012. <https://doi.org/10.1029/2012jc008055>
- Banse, K. (1959). On upwelling and bottom-trawling off the southwest coast of India. *Journal of the Marine Biological Association of India*, 1(1), 33–49.
- Banse, K., Naqvi, S., Narvekar, P., Postel, J., & Jayakumar, D. (2014). Oxygen minimum zone of the open Arabian Sea: Variability of oxygen and nitrite from daily to decadal timescales. *Biogeosciences*, 11(8), 2237–2261. <https://doi.org/10.5194/bg-10-15455-2013>
- Bianchi, D., Dunne, J. P., Sarmiento, J. L., & Galbraith, E. D. (2012). Data-based estimates of suboxia, denitrification, and N₂O production in the ocean and their sensitivities to dissolved O₂. *Global Biogeochemical Cycles*, 26(2), GB2009. <https://doi.org/10.1029/2011gb004209>
- Bianchi, D., Weber, T. S., Kiko, R., & Deutsch, C. (2018). Global niche of marine anaerobic metabolisms expanded by particle microenvironments. *Nature Geoscience*, 11(4), 263–268. <https://doi.org/10.1038/s41561-018-0081-0>
- Blondeau-Patissier, D., Gower, J. F., Dekker, A. G., Phinn, S. R., & Brando, V. E. (2014). A review of ocean color remote sensing methods and statistical techniques for the detection, mapping and analysis of phytoplankton blooms in coastal and open oceans. *Progress in Oceanography*, 123, 123–144. <https://doi.org/10.1016/j.pocean.2013.12.008>
- Boyer, T. P., Baranova, O. K., Coleman, C., Garcia, H. E., Grodsky, A., Locarnini, R. A., et al. (2018). NOAA Atlas NESDIS 87. World Ocean Database.
- Brandt, P., Bange, H. W., Banyte, D., Dengler, M., Didwischus, S.-H., Fischer, T., et al. (2015). On the role of circulation and mixing in the ventilation of oxygen minimum zones with a focus on the eastern tropical North Atlantic. *Biogeosciences*, 12(2), 489–512. <https://doi.org/10.5194/bg-12-489-2015>
- Breitburg, D., Levin, L. A., Oschlies, A., Grégoire, M., Chavez, F. P., Conley, D. J., et al. (2018). Declining oxygen in the global ocean and coastal waters. *Science*, 359(6371), eaam7240. <https://doi.org/10.1126/science.aam7240>
- Cai, W., Yang, K., Wu, L., Huang, G., Santoso, A., Ng, B., et al. (2021). Opposite response of strong and moderate positive Indian Ocean Dipole to global warming. *Nature Climate Change*, 11(1), 27–32. <https://doi.org/10.1038/s41558-020-00943-1>
- Carruthers, J., Gogate, S., Naidu, J., & Laevastu, T. (1959). Shorewards upslope of the layer of minimum oxygen off Bombay: Its influence on marine biology, especially fisheries. *Nature*, 183(4668), 1084–1087. <https://doi.org/10.1038/1831084a0>
- Clarke, A. J., & Liu, X. (1994). Interannual sea level in the northern and eastern Indian Ocean. *Journal of Physical Oceanography*, 24(6), 1224–1235. [https://doi.org/10.1175/1520-0485\(1994\)024<1224:isltn>2.0.co;2](https://doi.org/10.1175/1520-0485(1994)024<1224:isltn>2.0.co;2)
- Cui, Y., Wu, J., Ren, J., & Xu, J. (2019). Physical dynamics structures and oxygen budget of summer hypoxia in the Pearl River Estuary. *Limnology and Oceanography*, 64(1), 131–148. <https://doi.org/10.1002/leo.11025>
- Currie, J. C., Lengaigne, M., Vialard, J., Kaplan, D. M., Aumont, O., Naqvi, S., & Maury, O. (2013). Indian Ocean Dipole and El Niño/Southern Oscillation impacts on regional chlorophyll anomalies in the Indian Ocean. *Biogeosciences*, 10(10), 6677–6698. <https://doi.org/10.5194/bg-10-6677-2013>
- Decker, M. B., Breitburg, D. L., & Purcell, J. E. (2004). Effects of low dissolved oxygen on zooplankton predation by the ctenophore Mnemiopsis leidyi. *Marine Ecology Progress Series*, 280, 163–172. <https://doi.org/10.3354/meps280163>
- Deutsch, C., Penn, J. L., & Seibel, B. (2020). Metabolic trait diversity shapes marine biogeography. *Nature*, 585(7826), 557–562. <https://doi.org/10.1038/s41586-020-2721-y>
- Díaz, R. J., Rabalaïs, N. N., & Breitburg, D. L. (2010). Agriculture's impact on aquaculture: Hypoxia and eutrophication in marine waters. In *Advancing the aquaculture agenda: Workshop proceedings*. OECD Publishing.
- Díaz, R. J., & Rosenberg, R. (1995). Marine benthic hypoxia: A review of its ecological effects and the behavioural responses of benthic macrofauna. *Oceanography and Marine Biology: An Annual Review*, 33, 245–303.
- Díaz, R. J., & Rosenberg, R. (2008). Spreading dead zones and consequences for marine ecosystems. *Science*, 321(5891), 926–929. <https://doi.org/10.1126/science.1156401>
- Ekau, W., Auel, H., Pörtner, H.-O., & Gilbert, D. (2010). Impacts of hypoxia on the structure and processes in pelagic communities (zooplankton, macro-invertebrates and fish). *Biogeosciences*, 7(5), 1669–1699. <https://doi.org/10.5194/bg-7-1669-2010>
- Fennel, K., & Testa, J. M. (2019). Biogeochemical controls on coastal hypoxia. *Annual Review of Marine Science*, 11(1), 105–130. <https://doi.org/10.1146/annurev-marine-010318-095138>
- Garcia, H., Boyer, T., Baranova, O., Locarnini, R., Mishonov, A., Grodsky, A., et al. (2019). In A. Mishonov (Ed.), *World Ocean Atlas 2018: Product documentation*.

- Garrison, D. L., Gowing, M. M., Hughes, M. P., Campbell, L., Caron, D. A., Dennett, M. R., et al. (2000). Microbial food web structure in the Arabian Sea: A US JGOFS study. *Deep Sea Research Part II: Topical Studies in Oceanography*, 47(7–8), 1387–1422. [https://doi.org/10.1016/s0967-0645\(99\)00148-4](https://doi.org/10.1016/s0967-0645(99)00148-4)
- Geider, R., MacIntyre, H., & Kana, T. (1997). Dynamic model of phytoplankton growth and acclimation: Responses of the balanced growth rate and the chlorophyll-a: Carbon ratio to light, nutrient-limitation and temperature. *Marine Ecology Progress Series*, 148, 187–200. <https://doi.org/10.3354/meps148187>
- George, R., Muraleedharan, K., Martin, G., Sabu, P., Gerson, V. J., Dineshkumar, P., et al. (2013). Nutrient biogeochemistry of the eastern Arabian Sea during the southwest monsoon retreat. *Environmental Earth Sciences*, 68(3), 703–718. <https://doi.org/10.1007/s12665-012-1772-2>
- Gilbert, D., Rabalais, N. N., Diaz, R., & Zhang, J. (2010). Evidence for greater oxygen decline rates in the coastal ocean than in the open ocean. *Biogeosciences*, 7(7), 2283–2296. <https://doi.org/10.5194/bg-7-2283-2010>
- Gireeshkumar, T., Mathew, D., Pratihary, A., Naik, H., Narvekar, K., Araujo, J., et al. (2017). Influence of upwelling induced near shore hypoxia on the Alappuzha mud banks, South West Coast of India. *Continental Shelf Research*, 139, 1–8. <https://doi.org/10.1016/j.csr.2017.03.009>
- Glaspie, C. N., Clouse, M., Huebert, K., Ludsin, S. A., Mason, D. M., Pierson, J. J., et al. (2019). Fish diet shifts associated with the northern Gulf of Mexico hypoxic zone. *Estuaries and Coasts*, 42(8), 2170–2183. <https://doi.org/10.1007/s12237-019-00626-x>
- Gray, J. S., Wu, R. S.-S., & Or, Y. Y. (2002). Effects of hypoxia and organic enrichment on the coastal marine environment. *Marine Ecology Progress Series*, 238, 249–279. <https://doi.org/10.3354/meps238249>
- Gupta, G., Jyothibabu, R., Ramu, C. V., Reddy, A. Y., Balachandran, K., Sudheesh, V., et al. (2021). The world's largest coastal deoxygenation zone is not anthropogenically driven. *Environmental Research Letters*, 16(5), 054009. <https://doi.org/10.1088/1748-9326/abe9eb>
- Gupta, G., Sudheesh, V., Sudharma, K., Saravanan, N., Dhanya, V., Dhanya, K., et al. (2016). Evolution to decay of upwelling and associated biogeochemistry over the southeastern Arabian Sea shelf. *Journal of Geophysical Research: Biogeosciences*, 121(1), 159–175. <https://doi.org/10.1002/2015jg003163>
- Han, W., & Webster, P. J. (2002). Forcing mechanisms of sea level interannual variability in the Bay of Bengal. *Journal of Physical Oceanography*, 32(1), 216–239. [https://doi.org/10.1175/1520-0485\(2002\)032<0216:fmosli>2.0.co;2](https://doi.org/10.1175/1520-0485(2002)032<0216:fmosli>2.0.co;2)
- Helly, J. J., & Levin, L. A. (2004). Global distribution of naturally occurring marine hypoxia on continental margins. *Deep Sea Research Part I: Oceanographic Research Papers*, 51(9), 1159–1168. <https://doi.org/10.1016/j.dsr.2004.03.009>
- Jaleel, K. A., Kumar, P. A., Khan, K. N., Correya, N. S., Jacob, J., Philip, R., et al. (2014). Polychaete community structure in the south eastern Arabian Sea continental margin (200–1000 m). *Deep Sea Research Part I: Oceanographic Research Papers*, 93, 60–71. <https://doi.org/10.1016/j.dsr.2014.07.006>
- Jaleel, K. A., Parameswaran, U. V., Gopal, A., Khader, C., Ganesh, T., Sanjeevan, V., et al. (2015). Evaluation of changes in macrobenthic standing stock and polychaete community structure along the south eastern Arabian Sea shelf during the monsoon trawl-ban. *Continental Shelf Research*, 102, 9–18. <https://doi.org/10.1016/j.csr.2015.04.011>
- Jaleel, K. A., Parameswaran, U. V., Gopal, A., Khader, C., Sanjeevan, V., Vijayan, A. K., & Gupta, G. (2021). Response of macrozoobenthic communities to summer monsoon upwelling and related hypoxia in the south eastern Arabian Sea shelf. *Marine Environmental Research*, 166, 105278. <https://doi.org/10.1016/j.marenvres.2021.105278>
- Koné, V., Aumont, O., Lévy, M., & Resplandy, L. (2009). Physical and biogeochemical controls of the phytoplankton seasonal cycle in the Indian Ocean: A modeling study. *Indian Ocean Biogeochemical Processes and Ecological Variability*, 185, 350.
- Lachkar, Z., Smith, S., Lévy, M., & Pauluis, O. (2016). Eddies reduce denitrification and compress habitats in the Arabian Sea. *Geophysical Research Letters*, 43(17), 9148–9156. <https://doi.org/10.1002/2016gl069876>
- Laffoley, D., & Baxter, J. M. (2019). *Ocean deoxygenation: Everyone's problem-causes, impacts, consequences and solutions*. IUCN Gland.
- Laruelle, G. G., Landschützer, P., Gruber, N., Tison, J.-L., Delille, B., & Regnier, P. (2017). Global high-resolution monthly pCO₂ climatology for the coastal ocean derived from neural network interpolation. *Biogeosciences*, 14(19), 4545–4561. <https://doi.org/10.5194/bg-14-4545-2017>
- Levin, L., Ekau, W., Gooday, A., Jorissen, F., Middelburg, J., Naqvi, S., et al. (2009). Effects of natural and human-induced hypoxia on coastal benthos. *Biogeosciences*, 6(10), 2063–2098. <https://doi.org/10.5194/bg-6-2063-2009>
- Levitus, S., Antonov, J. I., Boyer, T. P., Locarnini, R. A., Garcia, H. E., & Mishonov, A. V. (2009). Global ocean heat content 1955–2008 in light of recently revealed instrumentation problems. *Geophysical Research Letters*, 36(7), L07608. <https://doi.org/10.1029/2008gl037155>
- Lévy, M., Shankar, D., André, J.-M., Shenoi, S., Durand, F., & de Boyer Montégut, C. (2007). Basin-wide seasonal evolution of the Indian Ocean's phytoplankton blooms. *Journal of Geophysical Research*, 112(C12), C12014. <https://doi.org/10.1029/2007jc004090>
- Llanillo, P., Pelegrí, J. L., Talley, L., Peña-Izquierdo, J., & Cordero, R. (2018). Oxygen pathways and budget for the eastern South Pacific Oxygen Minimum Zone. *Journal of Geophysical Research: Oceans*, 123(3), 1722–1744. <https://doi.org/10.1002/2017jc013509>
- Long, M. H., Rheuban, J. E., McCorkle, D. C., Burdige, D. J., & Zimmerman, R. C. (2019). Closing the oxygen mass balance in shallow coastal ecosystems. *Limnology and Oceanography*, 64(6), 2694–2708. <https://doi.org/10.1002/limo.11248>
- Lumban-Gaol, J., Siswanto, E., Mahapatra, K., Natih, N. M. N., Nurjaya, I. W., Hartanto, M. T., et al. (2021). Impact of the strong downwelling (upwelling) on small pelagic fish production during the 2016 (2019) negative (positive) Indian Ocean Dipole events in the Eastern Indian Ocean off Java. *Climate*, 9(2), 29. <https://doi.org/10.3390/cli9020029>
- Martin, G., Muraleedharan, K., Vijay, J., Rejomon, G., Madhu, N., Shivaprasad, A., et al. (2010). Formation of anoxia and denitrification in the bottom waters of a tropical estuary, southwest coast of India. *Biogeosciences Discussions*, 7(2), 1751–1782.
- Martin, G., Vijay, J., Laluraj, C., Madhu, N., Joseph, T., Nair, M., et al. (2008). Fresh water influence on nutrient stoichiometry in a tropical estuary, southwest coast of India. *Applied Ecology and Environmental Research*, 6(1).
- McCreary, J. P., Han, W., Shankar, D., & Shetye, S. R. (1996). Dynamics of the east India coastal current: 2. Numerical solutions. *Journal of Geophysical Research*, 101(C6), 13993–14010. <https://doi.org/10.1029/96jc00560>
- McCreary, J. P., Jr., Kundu, P. K., & Molinari, R. L. (1993). A numerical investigation of dynamics, thermodynamics and mixed-layer processes in the Indian Ocean. *Progress in Oceanography*, 31(3), 181–244. [https://doi.org/10.1016/0079-6611\(93\)90002-u](https://doi.org/10.1016/0079-6611(93)90002-u)
- Naqvi, S. W. A., DeSousa, S., Fondevilar, S., & Reddy, C. (1979). Distribution of dissolved oxygen in the western Bay of Bengal. *Mahasagar*, 12(1), 25–34.
- Naqvi, S. W. A., Jayakumar, D., Narvekar, P., Naik, H., Sarma, V., D'souza, W., et al. (2000). Increased marine production of N₂O due to intensifying anoxia on the Indian continental shelf. *Nature*, 408(6810), 346–349. <https://doi.org/10.1038/35042551>
- Naqvi, S. W. A., Naik, H., Jayakumar, A., Pratihary, A. K., Narvenkar, G., Kurian, S., et al. (2009). Seasonal anoxia over the western Indian continental shelf. *Indian Ocean Biogeochemical Processes and Ecological Variability*, 185, 333–345. <https://doi.org/10.1029/2008GM000745>
- Naqvi, S. W. A., Naik, H., Jayakumar, D., Shailaja, M., & Narvekar, P. (2006). Seasonal oxygen deficiency over the western continental shelf of India. In *Past and present water column anoxia* (Vol. 64, pp. 195–224). Springer.
- Naqvi, S. W. A., Naik, H., Pratihary, A., DeSouza, W., Narvekar, P., Jayakumar, D., et al. (2006). Coastal versus open-ocean denitrification in the Arabian Sea. *Biogeosciences*, 3(4), 621–633. <https://doi.org/10.5194/bg-3-621-2006>

- NASA Ocean Biology Processing Group (OBPG), & Stumpf, R. (2012). *Distance to nearest coastline: 0.01-degree grid: Ocean*. Distributed by the Pacific Islands Ocean Observing System (PacIOOS). Retrieved from http://pacioos.org/metadata/dist2coast_1deg_ocean.html
- Nestlerode, J. A., & Diaz, R. J. (1998). Effects of periodic environmental hypoxia on predation of a tethered polychaete, *Glycera americana*: Implications for trophic dynamics. *Marine Ecology Progress Series*, 172, 185–195. <https://doi.org/10.3354/meps172185>
- Nienhaus, M. J., Subrahmanyam, B., & Murty, V. S. N. (2012). Altimetric observations and model simulations of coastal Kelvin waves in the Bay of Bengal. *Marine Geodesy*, 35(sup1), 190–216. <https://doi.org/10.1080/01490419.2012.718607>
- Nigam, T., Pant, V., & Prakash, K. R. (2018). Impact of Indian Ocean Dipole on the coastal upwelling features off the southwest coast of India. *Ocean Dynamics*, 68(6), 663–676. <https://doi.org/10.1007/s10236-018-1152-x>
- Nixon, S. W. (1995). Coastal marine eutrophication: A definition, social causes, and future concerns. *Ophelia*, 41(1), 199–219. <https://doi.org/10.1080/00785236.1995.10422044>
- Norkko, J., Gammal, J., Hewitt, J. E., Josefson, A. B., Carstensen, J., & Norkko, A. (2015). Seafloor ecosystem function relationships: In situ patterns of change across gradients of increasing hypoxic stress. *Ecosystems*, 18(8), 1424–1439. <https://doi.org/10.1007/s10021-015-9909-2>
- Padmakumar, K., Thomas, L. C., Vijayan, A., & Sudhakar, M. (2016). “Crab Jubilee” subsequent to red tide of *Noctiluca scintillans* along the central Kerala coast (*SW coast of India*). *Paraswaran, U. V., Jaleel, K. A., Sanjeevan, V., Gopal, A., Vijayan, A. K., Gupta, G., & Sudhakar, M. (2018). Diversity and distribution of echinoderms in the South Eastern Arabian Sea shelf under the influence of seasonal hypoxia. *Progress in Oceanography*, 165, 189–204. https://doi.org/10.1016/j.pocean.2018.06.005*
- Piontovski, S., & Al-Oufi, H. (2015). The Omani shelf hypoxia and the warming Arabian Sea. *International Journal of Environmental Studies*, 72(2), 256–264. <https://doi.org/10.1080/00207233.2015.1012361>
- Poddar, S., Chacko, N., & Swain, D. (2019). Estimation of chlorophyll-a in northern coastal Bay of Bengal using Landsat-8 OLI and Sentinel-2 MSI sensors. *Frontiers in Marine Science*, 6, 598. <https://doi.org/10.3389/fmars.2019.00598>
- Prasanna Kumar, S., Muraleedharan, P., Prasad, T., Gauns, M., Ramaiah, N., De Souza, S., et al. (2002). Why is the Bay of Bengal less productive during summer monsoon compared to the Arabian Sea? *Geophysical Research Letters*, 29(24), 88-1–88-4. <https://doi.org/10.1029/2002gl016013>
- Rabalais, N., Diaz, R. J., Levin, L., Turner, R., Gilbert, D., & Zhang, J. (2010). Dynamics and distribution of natural and human-caused hypoxia. *Biogeosciences*, 7(2), 585–619. <https://doi.org/10.5194/bg-7-585-2010>
- Rao, R., Kumar, M. G., Ravichandran, M., Rao, A., Gopalakrishna, V., & Thadathil, P. (2010). Interannual variability of Kelvin wave propagation in the wave guides of the equatorial Indian Ocean, the coastal Bay of Bengal and the southeastern Arabian Sea during 1993–2006. *Deep Sea Research Part I: Oceanographic Research Papers*, 57(1), 1–13. <https://doi.org/10.1016/j.dsr.2009.10.008>
- Rao, S. A., & Behera, S. K. (2005). Subsurface influence on SST in the tropical Indian Ocean: Structure and interannual variability. *Dynamics of Atmospheres and Oceans*, 39(1–2), 103–135. <https://doi.org/10.1016/j.dynatmoco.2004.10.014>
- Rao, S. A., Behera, S. K., Masumoto, Y., & Yamagata, T. (2002). Interannual subsurface variability in the tropical Indian Ocean with a special emphasis on the Indian Ocean Dipole. *Deep Sea Research Part II: Topical Studies in Oceanography*, 49(7–8), 1549–1572. [https://doi.org/10.1016/s0967-0645\(01\)00158-8](https://doi.org/10.1016/s0967-0645(01)00158-8)
- Resplandy, L., Lévy, M., Bopp, L., Echevin, V., Pous, S., Sarma, V., & Kumar, D. (2012). Controlling factors of the oxygen balance in the Arabian Sea’s OMZ. *Biogeosciences*, 9(12), 5095–5109. <https://doi.org/10.5194/bg-9-5095-2012>
- Riedel, B., Zuschin, M., Haselmair, A., & Stachowitzsch, M. (2008). Oxygen depletion under glass: Behavioural responses of benthic macrofauna to induced anoxia in the Northern Adriatic. *Journal of Experimental Marine Biology and Ecology*, 367(1), 17–27. <https://doi.org/10.1016/j.jembe.2008.08.007>
- Rixen, T., Cowie, G., Gaye, B., Goes, J., do Rosário Gomes, H., Hood, R. R., et al. (2020). Reviews and syntheses: Present, past, and future of the oxygen minimum zone in the northern Indian Ocean. *Biogeosciences*, 17(23), 6051–6080. <https://doi.org/10.5194/bg-17-6051-2020>
- Roman, M. R., Brandt, S. B., Houde, E. D., & Pierson, J. J. (2019). Interactive effects of hypoxia and temperature on coastal pelagic zooplankton and fish. *Frontiers in Marine Science*, 6, 139. <https://doi.org/10.3389/fmars.2019.00139>
- Saji, N., Goswami, B., Vinayachandran, P., & Yamagata, T. (1999). A dipole mode in the tropical Indian Ocean. *Nature*, 401(6751), 360–363. <https://doi.org/10.1038/43854>
- Samir, K., & Lutz, W. (2017). The human core of the shared socioeconomic pathways: Population scenarios by age, sex and level of education for all countries to 2100. *Global Environmental Change*, 42, 181–192. <https://doi.org/10.1016/j.gloenvcha.2014.06.004>
- Sarkar, A., Naqvi, S. W. A., Lavik, G., Prathihary, A., Naik, H., Shirodkar, G., & Kuypers, M. M. (2020). Massive nitrogen loss over the western Indian continental shelf during seasonal anoxia: Evidence from isotope pairing technique. *Frontiers in Marine Science*, 7, 678. <https://doi.org/10.3389/fmars.2020.00678>
- Sathyendranath, S., Brewin, R. J., Brockmann, C., Brotas, V., Calton, B., Chuprin, A., et al. (2019). An ocean-colour time series for use in climate studies: The experience of the ocean-colour climate change initiative (OC-CCI). *Sensors*, 19(19), 4285. <https://doi.org/10.3390/s19194285>
- Satpathy, K., Panigrahi, S., Mohanty, A., Sahu, G., Acharya, M., Bramha, S., et al. (2013). Severe oxygen depletion in the shallow regions of the Bay of Bengal off Tamil Nadu coast. *Current Science*, 104(11), 1467–1469.
- Seitzinger, S., Mayorga, E., Bouwman, A., Kroese, C., Beusen, A., Billen, G., et al. (2010). Global river nutrient export: A scenario analysis of past and future trends. *Global Biogeochemical Cycles*, 24(4). <https://doi.org/10.1029/2009gb003587>
- Shetye, S. R. (1998). West India coastal current and Lakshadweep high/low. *Sadhana*, 23(5), 637–651. <https://doi.org/10.1007/bf02744586>
- Shirodkar, G., Naqvi, S. W. A., Naik, H., Prathihary, A. K., Kurian, S., & Shenoy, D. M. (2018). Methane dynamics in the shelf waters of the west coast of India during seasonal anoxia. *Marine Chemistry*, 203, 55–63. <https://doi.org/10.1016/j.marchem.2018.05.001>
- Sinha, E., Michalak, A., & Balaji, V. (2017). Eutrophication will increase during the 21st century as a result of precipitation changes. *Science*, 357(6349), 405–408. <https://doi.org/10.1126/science.aan2409>
- Stramma, L., Schmidtko, S., Levin, L. A., & Johnson, G. C. (2010). Ocean oxygen minima expansions and their biological impacts. *Deep Sea Research Part I: Oceanographic Research Papers*, 57(4), 587–595. <https://doi.org/10.1016/j.dsr.2010.01.005>
- Sudheesh, V., Gupta, G., Sudharma, K., Naik, H., Shenoy, D., Sudhakar, M., & Naqvi, S. (2016). Upwelling intensity modulates N₂O concentrations over the western Indian shelf. *Journal of Geophysical Research: Oceans*, 121(12), 8551–8565. <https://doi.org/10.1002/2016jc012166>
- Suresh, I., Vialard, J., Izumo, T., Lengaigne, M., Han, W., McCreary, J., & Muraleedharan, P. M. (2016). Dominant role of winds near Sri Lanka in driving seasonal sea level variations along the west coast of India. *Geophysical Research Letters*, 43(13), 7028–7035. <https://doi.org/10.1002/2016gl069976>
- Suresh, I., Vialard, J., Lengaigne, M., Izumo, T., Parvathi, V., & Muraleedharan, P. M. (2018). Sea level interannual variability along the west coast of India. *Geophysical Research Letters*, 45(22), 12–440. <https://doi.org/10.1029/2018gl080972>
- Thambithurai, D., Crespel, A., Norin, T., Rácz, A., Lindström, J., Parsons, K. J., & Killen, S. S. (2019). Hypoxia alters vulnerability to capture and the potential for trait-based selection in a scaled-down trawl fishery. *Conservation Physiology*, 7(1), coz082. <https://doi.org/10.1093/conphys/coz082>

- Thompson, P. R., Piecuch, C. G., Merrifield, M. A., McCreary, J. P., & Firing, E. (2016). Forcing of recent decadal variability in the Equatorial and North Indian Ocean. *Journal of Geophysical Research: Oceans*, 121(9), 6762–6778. <https://doi.org/10.1002/2016jc012132>
- Vallivattathillam, P., Iyyappan, S., Lengaigne, M., Ethé, C., Vialard, J., Levy, M., et al. (2017). Positive Indian Ocean Dipole events prevent anoxia off the west coast of India. *Biogeosciences*, 14(6), 1541–1559. <https://doi.org/10.5194/bg-14-1541-2017>
- Vaquer-Sunyer, R., & Duarte, C. M. (2008). Thresholds of hypoxia for marine biodiversity. *Proceedings of the National Academy of Sciences*, 105(40), 15452–15457. <https://doi.org/10.1073/pnas.0803833105>
- Vic, C., Capet, X., Roullet, G., & Carton, X. (2017). Western boundary upwelling dynamics off Oman. *Ocean Dynamics*, 67(5), 585–595. <https://doi.org/10.1007/s10236-017-1044-5>
- Villnäs, A., Norkko, J., Hietanen, S., Josefson, A. B., Lukkari, K., & Norkko, A. (2013). The role of recurrent disturbances for ecosystem multi-functionality. *Ecology*, 94(10), 2275–2287. <https://doi.org/10.1890/12-1716.1>
- Vinayachandran, P. N. M., Masumoto, Y., Roberts, M. J., Huggett, J. A., Halo, I., Chatterjee, A., et al. (2021). Reviews and syntheses: Physical and biogeochemical processes associated with upwelling in the Indian Ocean. *Biogeosciences*, 18(22), 5967–6029. <https://doi.org/10.5194/bg-18-5967-2021>
- Virtanen, P., Gommers, R., Oliphant, T. E., Haberland, M., Reddy, T., Cournapeau, D., et al. (2020). SciPy 1.0: Fundamental algorithms for scientific computing in Python. *Nature Methods*, 17(3), 261–272. <https://doi.org/10.1038/s41592-019-0686-2>
- Webster, P. J., Moore, A. M., Loschnigg, J. P., & Leben, R. R. (1999). Coupled ocean–atmosphere dynamics in the Indian Ocean during 1997–98. *Nature*, 401(6751), 356–360. <https://doi.org/10.1038/43848>
- Wiggert, J. D., Hood, R., Banse, K., & Kindle, J. (2005). Monsoon-driven biogeochemical processes in the Arabian Sea. *Progress in Oceanography*, 65(2–4), 176–213. <https://doi.org/10.1016/j.pocean.2005.03.008>
- Wiggert, J. D., Vialard, J., & Behrenfeld, M. J. (2009). Basinwide modification of dynamical and biogeochemical processes by the positive phase of the Indian Ocean Dipole during the SeaWiFS era. *Indian Ocean Biogeochemical Processes and Ecological Variability*, 185, 350. <https://doi.org/10.1029/2008GM000776>
- Wu, R. S. (2002). Hypoxia: From molecular responses to ecosystem responses. *Marine Pollution Bulletin*, 45(1), 35–45. [https://doi.org/10.1016/s0025-326x\(02\)00061-9](https://doi.org/10.1016/s0025-326x(02)00061-9)
- Yang, J., Yu, L., Koblinsky, C. J., & Adamec, D. (1998). Dynamics of the seasonal variations in the Indian Ocean from TOPEX/POSEIDON sea surface height and an ocean model. *Geophysical Research Letters*, 25(11), 1915–1918. <https://doi.org/10.1029/98gl01401>
- Yoann, T., Flye-Sainte-Marie, J., Chabot, D., Aguirre-Velarde, A., Marques, G. M., & Pecquerie, L. (2019). Effects of hypoxia on metabolic functions in marine organisms: Observed patterns and modelling assumptions within the context of Dynamic Energy Budget (DEB) theory. *Journal of Sea Research*, 143, 231–242. <https://doi.org/10.1016/j.seares.2018.05.001>
- Young, I. T. (1977). Proof without prejudice: Use of the Kolmogorov-Smirnov test for the analysis of histograms from flow systems and other sources. *Journal of Histochemistry and Cytochemistry*, 25(7), 935–941. <https://doi.org/10.1177/25.7.894009>
- Yu, W., Xiang, B., Liu, L., & Liu, N. (2005). Understanding the origins of interannual thermocline variations in the tropical Indian Ocean. *Geophysical Research Letters*, 32(24), L24706. <https://doi.org/10.1029/2005gl024327>